



Published in final edited form as:

Mol Cancer Res. 2018 May ; 16(5): 909–919. doi:10.1158/1541-7786.MCR-17-0597.

Autophagic Flux is Regulated by Interaction Between the C-terminal Domain of Patched1 and ATG101

Lucy X. Chen¹, Cintli C. Morales-Alcala², and Natalia A. Riobo-Del Galdo^{1,2,3}

¹Department of Biochemistry and Molecular Biology, Thomas Jefferson University, Philadelphia, PA19107, United States

²Leeds Institute of Cancer and Pathology, University of Leeds, Leeds, LS7 9TF, United Kingdom

³School of Molecular and Cellular Biology, University of Leeds, Leeds, LS7 9TF, United Kingdom

Abstract

The Hedgehog (Hh) receptor Patched1 (PTCH1) is a well-known tumor suppressor that in its active form represses Smoothened (SMO) activity, inhibits proliferation, and induces apoptosis. The cytoplasmic C-terminal domain (CTD) regulates PTCH1 turnover and nucleates a pro-apoptotic complex. In this study, it was mechanistically determined that Autophagy Related 10 (ATG101), essential for mammalian autophagy, physically interacts with the CTD of PTCH1 and connects it to the ULK complex, which stimulates the autophagy machinery in response to changes in nutrient availability. This interaction results in a blockade of basal autophagic flux and accumulation of autophagosomes with undegraded cargo. Remarkably, this function of PTCH1 is independent of its repressive activity on SMO, as shown in SMO-deficient cells or in the presence of a SMO inhibitor, but is opposed by Sonic Hedgehog (SHH). These findings reveal a novel non-canonical function of PTCH1 that limits autophagy, mediated by ATG101, which could have therapeutic implications in Hh-dependent cancers.

INTRODUCTION

The Hedgehog (HH) signaling pathway has essential functions in embryonic patterning, including cell fate specification, axon guidance, angiogenesis, and cell proliferation and survival (1, 2). Dysregulated activation of the HH pathway after birth can originate and/or promote cancer growth in many tissue types (3). The Hh ligands, Sonic, Indian, and Desert HH (SHH, IHH, DHH), bind to two closely related receptors, Patched1 and Patched2 (PTCH1 and PTCH2) (4, 5). In the absence of ligands, PTCH proteins repress Smoothened (SMO), a G protein-coupled-receptor superfamily member (6–8). Full activation of SMO occurs when HH ligands bind to and inhibit PTCH1/2 resulting in retention of SMO at the primary cilium and activation of GLI-dependent transcription, known as canonical HH signaling (5).

PTCH1 is the most important and widely expressed HH receptor, since its deficiency is embryonic lethal with phenotypes of ventralization and polydactyly and somatic loss-of-

Conflict of Interest: The authors declare no potential conflicts of interest.

function mutations induce formation of medulloblastoma and basal cell carcinoma in mice and humans (9, 10). PTCH1 protein has 12-transmembrane (TM) domains, cytosolic N- and C-terminal domains, and a large central cytosolic loop. The TM domains 4–6 encode a sterol sensing domain and the central region has homology with resistance-nodulation-division (RND) bacterial permeases. Both functional domains and the 12-TM “core” are necessary for inhibition of SMO in the absence of HH proteins. The PTCH1 CTD is dispensable for regulation of SMO (11); however, it is a critical regulatory domain responsible for the high turnover rate of PTCH1 (12, 13). The CTD binds to the ubiquitin E3 ligase Itch, which catalyzes ubiquitylation of K1426 to induce endocytosis and degradation of PTCH1 (13). Limiting the expression level of PTCH1 is relevant because a region of the CTD adjacent to the Itch-binding PPXY site interacts with the adaptor proteins DRAL and TUCAN1 and induces the nucleation and activation of procaspase-9, leading to apoptotic cell death (14). This pro-apoptotic function of PTCH1, which has been classified as a “dependence receptor” because SHH prevents this negative signaling (15), belongs to the so called “non-canonical” HH signaling pathways, as it is independent of SMO and of the activity of the GLI transcription factors (13, 16). Thus, while the core 12-TM of PTCH1 functions in the regulation of canonical HH signaling, the CTD can regulate cell survival through other mediators.

In this study, we sought to identify additional mediators of PTCH1 non-canonical signaling by screening a cDNA library for specific interactions with the CTD. We found an unexpected interaction with an autophagy-specific protein. Autophagy is the process of the self-degradation of damaged organelles, cytoplasmic components and misfolded protein aggregates by segregation into a double membrane vesicle, the autophagosome, and fusion with lysosomes for proteolysis and lipolysis to take place (17, 18). The initiation of autophagy requires the unc51-like autophagy activating kinase (ULK) complex, which contains the Ser/Thr kinases ULK1 or ULK2, the autophagy-related protein 13 (ATG13), the FAK family kinase-interacting protein of 200 kDa (FIP200) and the autophagy-related protein 101 (ATG101) (19). Nutrient starvation increases ULK kinase activity and causes phosphorylation of Beclin-1 and activation of the Vps34 subunit of an endomembrane-specific class III PI3K complex that generates phosphatidylinositol-3-phosphate (PI3P) (20). PI3P triggers recruitment of the ATG12–ATG5–ATG16L1 complex to the extending phagophore membrane, where it lipidates LC3BI to generate the autophagosome membrane-bound LC3BII, a commonly used marker of autophagy (20, 21). LC3BII associates with the internal and external autophagosome membranes as the isolation membrane expands to form the autophagosome that engulfs a portion of the cytosol or selected cargo and organelles to be degraded (19). The last step in autophagy is the fusion of the autophagosome with lysosomes to form autolysosomes. After fusion, the contents of the autophagosome, including LC3BII, are degraded to generate biosynthetic building blocks and/or to eliminate damaged organelles or dangerous protein aggregates.

Here, we report that in the absence of SHH, the CTD of PTCH1 interacts with the ULK complex through Atg101 and blocks completion of autophagy in a SMO-independent manner. We propose that the tumor suppressor function of PTCH1 relies on its regulation of the canonical Hh pathway as much as in the control of autophagy through CTD-dependent signaling.

MATERIALS AND METHODS

Reagents

Recombinant Shh was synthesized, purified, and tested as previously described. KAAD-cyclopamine was purchased from EMD Millipore (Billerica, MA). Bafilomycin A1, chloroquine, doxycycline, and anti- β -actin antibody (AC-74) were from Sigma-Aldrich (St. Louis, MO). Antibodies targeting HA(C29F4), myc (9B111), ATG101, p62, LC3B, FIP200, ULK1, phospho-ULK1(Ser757), ATG13, and GLI1 (L42B10) were from Cell Signaling Technology (Danvers, MA). Secondary anti-rabbit-HRP and anti-mouse-HRP antibodies were purchased from BioRad (Hercules, CA). Anti-GFP, secondary anti-rabbit-HRP and anti-mouse-HRP Alexa 488 and Alexa 568 antibodies were from Invitrogen (Waltham, MA).

Plasmids and adenoviral vectors

PTCH1-HA, *PTCH1 CTD-HA*, *PTCH1-myc*, and *myr-GFP-CTD1* encoding vectors were previously described (14). The myrGFP-CTD1 targets the fusion to the plasma membrane and endocytic vesicles. *ATG101-RFP* and *HA-ATG101* (in PRK5 backbone) plasmids were a generous gift from Dr. Carol Mercer (University of Cincinnati, OH). AdV-*PTCH1-HA* was previously described (14).

Cell Culture

HEK 293, and HeLa cells were from American Type Tissue Collection (ATCC), *Smo*^{-/-} MEFs were a gift from Dr. James Chen (Stanford University) and *Ptc1*^{-/-} MEFs were a gift from Dr. Matthew Scott (Stanford University). Cells purchased from ATCC were not further authenticated, while the genotype of *Smo*^{-/-}, *Ptc1*^{-/-} and *Ptc1*^{+/-} MEFs was verified by PCR. HEK293 and HeLa cells were used between passages 2–15 after thawing, while MEFs were used between 2–8 passages. Cells were tested for the presence of mycoplasma every 6 months by PCR analysis of conditioned medium of high density cultures. To generate *SmoM2* cells in the *Smo*^{-/-} background, *Smo*^{-/-} MEFs were transfected with *SmoM2* cloned into pcDNA3.1-hygro or with empty plasmid by the calcium phosphate method. Cells were selected with hygromycin and expression of SmoM2 was confirmed by western blot, as previously described (22). All cells were cultured in Dulbecco's modified Eagle medium with 10% fetal bovine serum (Life Technologies), 100 U/ml penicillin, and 100 μ g/ml streptomycin and maintained in a humidified 37 °C incubator at 5% CO₂.

HEK 293, HeLa, and *Ptc1*^{-/-} MEFs cells were transfected using Lipofectamine 2000 (Life Technologies, Camarillo, CA), following the manufacturers' instructions. *Smo*^{-/-} and *SmoM2* MEFs were transduced with adenoviral particles.

Yeast Two-Hybrid Analysis

The yeast two-hybrid screening was carried out by Creative BioLabs using the Matchmaker Gold Yeast Two-Hybrid System (Clontech). The bait construct for yeast two-hybrid screening was made by subcloning the cDNA encoding NM_008957 (PTCH1 3469–4305 (278AA)) into the vector pGBKT7 (Clontech). The bait construct was transformed into the strain Y2HGold (*MATa*, *trp1-901*, *leu2-3, 112*, *ura3-52*, *his3-200*, *gal4*, *gal80*, *LYS2* :: *GAL1*_{UAS}-*Gal1*_{TATA}-*His3*, *GAL2*_{UAS}-*Gal2*_{TATA}-*Ade2* *URA3* :: *MEL1*_{UAS}-*Mel1*_{TATA}

AURI-C MEL1) using standard procedures. The absence of autoactivation of the bait construct was verified by plating transformed yeast on minimal medium lacking the tryptophan and supplemented with X- α -galactosidase and Aureobasidin A. In the yeast two-hybrid screening, the bait was mated with Mouse Embryo 17-day Mate & Plate library (Clontech) into Y187 strain. In total, 7×10^6 hybrids were screened. The potential positive hybrids were tested for His and Ade activation by co-transformation into the Y2HGold yeast strain. 23 positive clones showed His/Ade activation. The identity of the positive interactors was determined by sequencing.

RNA interference

Silencer select negative control siRNA #1 (#4390843), *ATG101* siRNA-1 (#s34253) (sense 5'-ACUUCAUCGACUUCACUUAAtt-3'; antisense UAAGUGAAGUCGAUGAAGUca), *ATG101* siRNA-2 (#s34254) (sense 5'-CAGCCCUACCUGUACAAGAtt -3'; antisense UCUUGUACAGGUAGGGCUGca) were purchased from Ambion. Transfection was performed using 100nM of siRNA for HEK 293 cells, or 3nM for HeLa cells, using HiPerFect transfection reagent (Qiagen) according to the manufacturer's protocol.

Detection of autophagic markers by western blotting

Cells were seeded in 6-well plates transfected or virally transduced as indicated above. At the end of the experiment, the culture medium was removed, cells were washed once in ice-cold PBS, and directly lysed in 100 μ l of $1 \times$ Laemmli buffer (2% sodium dodecyl sulfate, 10% glycerol, 5% 2-mercaptoethanol, 0.002% bromphenol blue and 62.5 mM Tris HCl, pH 6.8) to recover all soluble and insoluble material. Whole cell lysates were then sonicated for 15 sec, heated 5 min at 95°C, and used immediately or stored at -20°C for up to 5 days. Samples were separated in 15% SDS-PAGE gels, transferred onto nitrocellulose membranes at 50V for 2 h, and probed with anti-LC3B, p62 and β -actin antibodies at 1:1,000 dilution, followed by HRP-conjugated-secondary antibodies at 1:2,000 dilution.

Immunoprecipitation

For immunoprecipitation (IP) or co-immunoprecipitation (co-IP), cells were lysed in IP lysis buffer (50 mM Tris, pH 7.5, 150 mM NaCl, 1% NP-40, 1 mM EDTA, 1 mM EGTA, 2.5 mM MgCl₂, 0.5% sodium deoxycholate, 1 mM DTT supplemented with protease inhibitors) for 30 min at 4°C. The lysate was cleared by centrifugation at 4°C. Antibodies were added as recommended by the manufacturer for 2 h, followed by incubation with protein-A Dynabeads (Invitrogen) for 1 h at 4°C. After three washes in lysis buffer, proteins were eluted in Laemmli buffer for Western Blot. Densitometric quantifications of protein were determined using Image J software and normalized to total protein loading.

Immunofluorescence

Cells were cultured and transfected on Lab-Tek II chamber slides. Cells were fixed for 15 min in 4% formaldehyde, washed with phosphate buffered saline (PBS) 3 times, and incubated in blocking buffer (PBS, 5% goat serum, 0.1% saponin) for 1h at room temperature. Primary antibody was diluted in antibody solution (PBS, 1% BSA, 0.1% saponin) and incubated at 4C overnight. After washed with PBS 3 times, cells were

incubated with secondary antibody conjugated with Alexa Fluor 488 or 568 (Invitrogen) for 1h at room temperature. After PBS wash, the slides were mounted with Prolong Gold Antifade reagent. The immunofluorescent pictures were taken by the Zeiss LSM510 Meta Confocal Laser Scanning Microscope or Nikon Eclipse E800, and analyzed by the LSM image browser or Nikon NIS Elements BR 3.0 software.

Live cell imaging

HEK 293 cells were infected with BacMam 2.0 RFP-GFP-LC3B (Invitrogen) for 24 hours followed by transfection with pcDNA3.1 or *PTCH1-HA* plasmids as described above. After 24 h, red and green LC3B⁺ vesicles were imaged and quantified by using a Nikon Spinning Disk Confocal Microscope and MetaMorph Premier image acquisition and analysis software. The percentage of red vesicles over red + green vesicles (representing % autolysosomes) was quantified in 5 different fields in 3 independent experiments.

Gli-luciferase assay—*Ptc1*^{-/-} MEFs were seeded in 24-well plates and transfected on the following day when they were at ~70% confluence. *PTCH1-HA* or empty vector, p8XGli-Luc, and pRL-TK were transfected at a ratio of 4:1:0.1 using the Fugene HD reagent according to the manufacturer's protocol. When cells reached 100% confluence, typically between 24 and 48 h after transfection, the medium was changed to 0.5% serum for an additional 24 h, and 0.5 μ M KAAD-cyclopamine added to some of the wells transfected with pcDNA3.1. Luciferase activity was determined with the Dual-Luciferase Reporter Assay System (Promega) using a Promega Glomax 20/20 luminometer, following the manufacturer's directions.

Quantitative PCR—Total RNA was isolated from cells using the RNeasy kit (Qiagen, Valencia, CA) as directed. cDNA was synthesized using the High Capacity cDNA Reverse Transcription kit (Applied Biosystems). Quantitative PCR of *p62* and *MAPI LC3B* was carried out using SsoFast EvaGreen Supermix (BioRad) and normalized to GAPDH. Primer sequences were as follows: *GAPDH* forward: 5'-CCCATCACCATCTTCCAGGAGCGA-3', reverse 5'-TCCACCCTTCAAGTGGGCCCC-3'; *MAPI LC3B* forward 5'-AGCAGCATCCAACCAAATC-3', reverse 5'-CTGTGTCCGTTACCAACAG-3' (23); *p62(SQSTM1)* forward 5'-ATCGGAGGATCCGAGTGT-3', reverse 5'-TGGCTGTGAGCTGCTCTT-3' (24). Data were analyzed by the 2^{-Ct} method.

Statistics—Densitometry of the protein levels on Western blots was performed using ImageJ software. Results were analyzed by a paired *t* test or by one-way analysis of variance, followed by Tukey's *post hoc* comparison or by a paired Student's *t* test, using GraphPad Prism (version 5.0) software

RESULTS

The C-terminal domain of Patched1 interacts with the autophagy protein ATG101

We used the yeast-two-hybrid technique to identify novel proteins that are able to physically interact with the CTD of PTCH1, which we reported previously influences cell survival independently of the canonical Hh pathway and is dispensable for repression of SMO. The

CTD of PTCH1 was fused to the GAL4 DNA-binding domain and used as bait to screen a mouse embryo E17 cDNA library cloned as fusions to GAL4-activator domain (prey). One of the complementing plasmids encoded a large fragment of Atg101(1–167), a mammalian-specific subunit of the ULK complex. Atg101 is almost entirely comprised of a single highly-structured Hop1, Rev7, Mad2 (HORMA) domain (1–198), followed by a short unstructured “safety belt” (199–218), which in other HORMA domain-containing proteins like Mad2 allows a switch between open and closed conformations (25, 26). Thus, almost the complete HORMA domain of Atg101 was able to interact with the CTD of PTCH1 in yeast (Fig. 1A). This interaction was confirmed in HEK 293 cells by coimmunoprecipitation of a plasma membrane-targeted CTD fused to GFP (myr-GFP-CTD1) and hemagglutinin (HA)-tagged ATG101 (Fig. 1B). The use of myristoylated GFP-CTD1 ruled out that the interaction the result of mislocalized CTD expression. The ability of full-length PTCH1 to interact with ATG101 was also confirmed by co-immunoprecipitation of myc-PTCH1 with HA-ATG101 (Fig. 1C). Confocal microscopy showed that co-expressed PTCH1-eGFP and ATG101-RFP have a large degree of colocalization, in agreement with the biochemical studies (Fig. 1D).

Patched1 interacts with the ULK complex through ATG101 HORMA domain

ATG101 is part of a >3 MDa complex containing ULK1/2, FIP200, and ATG13 that senses nutrient availability for the control of autophagy. Immunoprecipitation of PTCH1 was able to pulldown not only endogenous ATG101, but also the entire ULK complex in HEK293 (Fig. 2A) and HeLa cells (Fig. 2B). To investigate if interaction of PTCH1 with the ULK complex was mediated by ATG101, we silenced *ATG101* expression by siRNA. As shown in Fig. 2C, a reduction in ATG101 protein level of ~90% caused a strong reduction of associated ATG101, ATG13, and ULK1. Unexpectedly, FIP200 interaction was retained in Atg101 depleted cells, albeit at a lower level. FIP200 is a large coiled-coil protein that interacts with many different partners and our data suggests that it could associate with full length PTCH1 via an unknown domain. In summary, these findings demonstrate that PTCH1 is able to interact with the endogenous ULK autophagy initiation complex via the ATG101 HORMA domain, and possible through FIP200, suggesting a regulatory function on autophagy or nutrient sensing.

Patched1 inhibits basal and nutrient starvation-induced autophagy

We next sought to determine whether the interaction between PTCH1 and ATG101 has a functional consequence on autophagy. Autophagic flux is a dynamic process that describes the formation of autophagosomes containing cargo, their fusion with lysosomes, and final degradation of their content in the acidic environment of the autolysosomes. During initiation of autophagy, LC3BI is conjugated to phosphatidylethanolamine to form LC3BII, which marks autophagosome membranes. The internal membrane pool of LC3BII anchors adaptor proteins, such as p62, which link the cargo for degradation to the autophagosome lumen. After autolysosome formation, the internal pool of LC3BII and p62 are both degraded along with the cargo. Thus, during autophagy, LC3BII levels first increase and then decrease rapidly, while p62 levels only decrease. Measurement of the relative levels of those two markers at different time points serves as a surrogate of “autophagic flux”. A useful tool for the study of autophagic flux are the drugs bafilomycin A1 and chloroquine

that act by interfering with lysosomal fusion and acidification, increasing LC3BII and p62 levels. Overexpression of PTCH1 in cells growing in complete medium increased the level of LC3BII and p62, suggesting a similar mode of action to bafilomycin A1 (Fig.3A and 3B). Interestingly, LC3BI levels were also elevated in PTCH1-expressing cells (1.9 ± 0.2 -fold, $P < 0.05$), further supporting the notion that its degradation could be blocked. We ruled out that the increase of these markers was due to increased transcription because *p62* and *LC3B* mRNA levels in PTCH1-HA-transfected cells were reduced by 24% and 55 %, respectively, as determined by qPCR (Fig. 1S). Amino acid starvation in Earle's balanced salt solution (EBSS) for 4 h induced autophagy, as seen by reduction of both LC3BII and p62 compared cells grown in complete media, but strikingly less efficiently in cells overexpressing PTCH1 (Fig.3A and 3C). If the accumulation of LC3BII and p62 by PTCH1 were the result to a blockage at a step downstream autophagosome formation, addition of bafilomycin A1 or chloroquine would not cause further accumulation, while they would increase the level of the same markers in control cells. As shown in Fig. 3C, neither bafilomycin A1 nor chloroquine increased LC3BII and p62 levels in PTCH1-expressing cells. These findings suggest that PTCH1 overexpression in HEK 293 or HeLa cells seems to block autophagic flux, in contradiction with a previous study (27). Therefore, we used the tandem eGFP-RFP-LC3B reporter assay as a second independent measure of autophagic flux. Expression of the eGFP-RFP-LC3B reporter marks autophagosomes in green and red fluorescence, since they accumulate lipidated eGFP-RFP-LC3BII. However, as autophagy proceeds, autophagosomes fuse with lysosomes and the contents are acidified, leading to a strong selective decrease in GFP fluorescence. In this assay, overexpression of PTCH1 in complete growth medium statistically reduced the percentage of RFP-only vesicles (autolysosomes) from $11.3 \pm 2.7\%$ to $4.3 \pm 1.1\%$ (Fig. 3D).

In order to investigate the function of endogenous Patched1 in autophagy, we compared the autophagic flux under amino acid-starvation of mouse embryonic fibroblasts (MEFs) isolated from *Ptc1*^{-/-} mice or *Ptc1*^{+/-} littermates. While both genotypes expressed similar levels of p62 and LC3B, *Ptc1*^{-/-} MEFs increased LC3BII and p62 levels to a significantly larger degree than *Ptc1*^{+/-} MEFs after addition of bafilomycin A1 (Fig. 3E). In other words, *Ptc1*^{-/-} cells are more sensitive to the inhibitory actions of bafilomycin A1 compared to *Ptc1*^{+/-} cells, as expected if endogenous Ptc1 limited the rate of autophagy. In addition, expression of PTCH1-HA in *Ptc1*^{-/-} MEFs increased LC3BII and p62 levels (Fig. 3F). Altogether, these observations suggest that PTCH1, expressed ectopically or endogenously, reduces autophagic flux by reducing autolysosome formation or by preventing their acidification and, consequently, reducing cargo degradation.

The CTD of Patched1 is necessary to inhibit autophagy

Since PTCH1 associates with ATG101 through the CTD, we tested whether this domain was necessary for autophagy inhibition. Expression of a PTCH1 mutant lacking the entire C-tail (PTCH1 CTD) was unable to increase LC3BII and p62 levels (Fig. 4A). Quantification of LC3BII increase (Fig. 4B) and of p62 (Fig. 4C) revealed a ~3-fold for full length PTCH1 ($P < 0.05$) and less than 1.5-fold for the CTD-lacking protein (non-significant, $P > 0.1$) demonstrating that the effect is mostly mediated by the CTD. Conversely, we tested if the isolated CTD was sufficient to block autophagic flux. Overexpression of the isolated CTD

increased the levels of LC3BII and p62 in HeLa cells (Fig. 4D–F), but it did not affect the markers in HEK293 cells significantly (Fig. 2S). In summary, our results demonstrate that the CTD of PTCH1 is necessary for the autophagic block phenotype.

ATG101 depletion attenuates accumulation of LC3BII and p62 after PTCH1 overexpression

Since the CTD of PTCH1 interacts with ATG101, we sought to determine if ATG101 was a necessary mediator of autophagic flux inhibition by PTCH1. Silencing of *ATG101* with two different siRNA duplexes strongly reduced LC3BII and p62 increase by PTCH1, although not completely (Fig. 5A and B). While the findings can be explained by the well-known requirement of ATG101 for mammalian autophagy, it indicates that most of the autophagic phenotype of PTCH1 can be explained by its interaction with ATG101. Interestingly, PTCH1 levels significantly increase when *ATG101* gene expression is silenced (Fig. 5A), suggesting that PTCH1 might be degraded along with other cargoes during autophagy.

Patched1 function in autophagy is independent of Smoothened

The CTD of PTCH1 is dispensable for canonical Hh signaling (12, 14). Therefore, the requirement of the CTD for autophagic flux blockade suggests that this novel function of PTCH1 is independent of SMO regulation, i.e. through a type I non-canonical pathway. To test this hypothesis, we compared the effect of PTCH1 in mouse cells deficient in Smoothened (*Smo*^{-/-} MEFs), unable to signal through the canonical Hh pathway with the same cells rescued with a constitutively active Smo mutant (SmoM2). The basal expression of Gli1 is undetectable in *Smo*^{-/-} MEFs and is maximal in SmoM2-expressing cells (Fig. 6A). Importantly, the SmoM2 mutant is insensitive to regulation by PTCH1, as seen by its failure to inhibit Gli1 expression in those cells (Fig. 6A). Introduction of PTCH1 in SmoM2-expressing MEFs by adenoviral delivery resulted in an increased level of LC3BII and p62 (Fig. 6B, C), demonstrating that repression of SMO by PTCH1 is not required to inhibit autophagic flux. As a second approach to demonstrate that SMO is not a mediator of PTCH1-induced autophagy inhibition, we compared the effect of PTCH1 expression in HEK 293 cells cultured in the presence of vehicle or of KAAD-cyclopamine, a specific SMO inhibitor. Although LC3BII and p62 levels tended to be higher after KAAD-cyclopamine treatment for 24 h, expression of PTCH1 elicited a further increase comparable to the one in cells treated with vehicle (Fig. 6D, E). Under the same experimental conditions, expression of PTCH1 or addition of KAAD-cyclopamine fully inhibited a Gli-luciferase reporter in *Ptc1*^{-/-} MEFs (Fig. 6F). These findings demonstrate that PTCH1 inhibits autophagic flux independently of modulation of the canonical Hh pathway.

Sonic Hedgehog opposes autophagic flux blockade by PTCH1

Binding of SHH to PTCH1 activates the canonical HH pathway and inhibits PTCH1's proapoptotic activity, also mediated by the CTD (13, 14). Thus, we tested if SHH was also able to prevent autophagic blockage by the CTD of PTCH1 in HEK 293 cells. While PTCH1 alone increased LC3BII and p62, simultaneous expression of PTCH1 and SHH prevented the increase in both markers (Fig. 6G). It is worth noting that cells expressing SHH had lower PTCH1-HA protein levels (Fig. 6G), since SHH binding to PTCH1 increases its turnover rate (13) and PTCH1-HA is expressed at a constant rate from the CMV promoter of the pcDNA3.1 vector. In addition, a modest reduction in basal LC3BII and p62 levels was

observed by expression of SHH alone (Fig. 6G), although given the magnitude of the effect, it did not reach statistical significance. Since SHH both inhibits PTCH1 and induces its degradation, we cannot distinguish if SHH inhibits PTCH1 autophagic function directly or indirectly by reducing its levels. However, this data demonstrates that the inhibitory effect of PTCH1 on autophagy is prevented by Hh ligands.

DISCUSSION

The tumor suppressor role of PTCH1, the Hh proteins receptor, is exerted through regulation of several downstream targets. First and most critical, it represses the oncogene SMO and blocks induction of pro-survival and mitogenic Gli-target genes through the canonical Hh pathway. In this and in a previous study (14), we continue to identify novel functions of PTCH1 that oppose cell growth and survival and are independent of SMO. The CTD of PTCH1 is dispensable for repression of SMO, although it facilitates SMO activation by increasing PTCH1 turnover (13). The HECT domain-containing E3 ubiquitin ligase Itch binds to PTCH1 CTD and ubiquitylates K1413, inducing internalization and degradation (14). A different region of PTCH1 CTD, N-terminal of K1413, binds a protein complex containing pro-caspase-9 and activates an extrinsic apoptotic cascade that results in cell death and is sensitive to inhibition by Shh (15). Here we find a novel function of the CTD of PTCH1 that is exerted through physical interaction with the ULK complex subunit ATG101. Unbiased yeast two-hybrid screening using PTCH1 CTD was used to identify the HORMA domain of ATG101, a 25 kDa protein essential for ULK complex activation in mammals that acts as a chaperone for ATG13 (25). Our study validated the interaction with full-length PTCH1, through the CTD, in normal and transformed mammalian cells. Remarkably, PTCH1 interacts with all the proteins of the ULK complex (ULK1, ATG13, and FIP200) through its binding to ATG101. Downstream of the ULK complex, PTCH1 causes a reduction of the autophagic flux by a mechanism that resembles that of bafilomycin A1. Autophagic flux is a dynamic process that encompasses formation of phagophore membranes decorated with lipidated LC3B, closure into autophagosomes containing organelles and other cargo labelled with p62, fusion of the outer membrane of the autophagosome with lysosomes, and degradation by acidic hydrolases of the autolysosomal contents. Thus, increases in LC3BII levels by western blot or imaging can be explained by increased lipidation (autophagy induction) or decreased clearance by a blockade at the last steps of the process (fusion or acidification). Previously it was reported that PTCH1 expression increased LC3BII levels, which was interpreted as an increased in autophagy (27). We performed a series of controls to distinguish the two possibilities. First, blockade of autolysosomal acidification with bafilomycin A1 or chloroquine showed no difference in accumulated LC3BII in cells expressing PTCH1 vs. empty plasmid. Second, we used the tandem RFP-GFP-LC3B marker to distinguish acidic from neutral pH vesicles that reflects autolysosomes and autophagosomes, respectively, and observed a 75% reduction in acidic LC3B⁺ structures. Both sets of results indicate that PTCH1 causes a reduction of the autophagic flux at the step of fusion of autophagosomes with lysosomes or that it compromises their acidification. Our conclusions are supported by a previous report that *Ptc1*^{-/-} MEFs, with constitutive Hh signalling, have an increased autophagic flux than wild type cells, as we confirmed in this study. In that report, the authors also show that

stimulation of SMO downstream of PTCH1 increases autophagic flux, but did not evaluate the effect of activation of HH signalling by the physiological SHH ligand. Our study and that of Pampliega *et al.* suggest that SHH increases autophagy by a double mechanism requiring suppression of the autophagy block imposed by PTCH1 and activation of a pro-autophagic signal from SMO (28).

Upon activation, the ULK complex relocates to perinuclear membranes to stimulate the class III PI3K complex composed of Vps34, Vps15, Beclin, AMBRA1 and other regulatory subunits. Production of phosphatidylinositol-3-phosphate is a critical signal for membrane nucleation during autophagosomes formation. The process of autolysosome formation involves the activity of two additional class III PI3K complexes, the UVRAG complex and the Rubicon complex. Their opposing activity promotes (UVRAG) and inhibits (Rubicon) fusion and completion of autophagy (19; 29). PTCH1 could be acting on one of these complexes or perhaps directly preventing acidification. It has been proposed, based on homology to bacterial permeases of the resistance-nodulation-differentiation (RND) family, that PTCH1 might function as a transporter of small lipophilic compounds in exchange for H⁺ (30). Thus, it is plausible that PTCH1 opposes lysosomal acidification independently of its interaction with ATG101, as suggested by the residual p62 accumulation in ATG101-depleted cells.

The biological relevance of our findings is in line with our knowledge of PTCH1 in cancer. First, *PTCH1* expression is very low in the absence of Shh, since it is one of the principal GLI-target genes. Second, PTCH1 is a dependence receptor and if overexpressed in the absence of ligand it triggers caspase-9-dependent apoptosis. Here we show that overexpression of PTCH1 in the absence of ligand also blocks autophagic flux and it does so through interaction with ATG101. All these functions of PTCH1 result in diminished fitness for cancer cells. Somatic *Ptch1* mutations in basal cell carcinomas frequently result in premature truncation of the CTD, which have also been detected in endometrial, colorectal, and gastric adenocarcinomas (31, and Cancer Genome Atlas TGCA Database). We propose that premature truncation of the CTD enhances cancer cell survival by avoidance of PTCH1-induced apoptosis and autophagy blockade. Moreover, many epithelial cancers of the GI tract with upregulated Hh signalling but without PTCH1 mutations are addicted to high levels of Shh or Ihh, and it is tempting to speculate that in part this is due to the required constant inhibition of PTCH1 to restraint the pro-apoptotic and anti-autophagic signalling. It is not surprising, then, that SMO inhibitors have failed in trials to prevent GI tract neoplasms progression.

Our findings also clearly demonstrate that this novel function of PTCH1 is independent of SMO and Gli-dependent transcription. However, some canonical Gli-target genes have been shown to regulate autophagy (27), suggesting that the Hh pathway is able to regulate autophagy in different manners: in the absence of ligand, PTCH1 actively represses autophagy through a non-canonical pathway mediated by ATG101, while, in the presence of Hh proteins, PTCH1 is inhibited and pro-autophagic target genes are induced downstream of SMO by activation of the GLI transcription factors.

In conclusion, we identify a novel function of the Hh receptor PTCH1 in the regulation of autophagy that is mediated by physical interaction of its CTD with the ULK complex through ATG101. Inhibition of autophagy by PTCH1 is not the result of SMO repression, and it supports the need for development of therapeutic biologicals that block binding of PTCH1 to Hh ligands to promote cancer cell death.

Supplementary Material

Refer to Web version on PubMed Central for supplementary material.

Acknowledgments

We thank Matthew Campbell and Steven Peeke for their technical help with the yeast-2-hybrid analysis of positive clones. This work was funded by the National Institutes of Health grant RO1 GM088256 to Natalia A. Riobo and CONACYT Mexican external studentship to Cintli Morales-Alcala.

References

1. Ingham PW, McMahon AP. Hedgehog signalling in animal development: paradigms and principles. *Genes Dev.* 2001; 15:3059–87. [PubMed: 11731473]
2. Martí E, Bovolenta P. Sonic Hedgehog in CNS development: one signal, multiple outputs. *Trends Neurosci.* 2002; 25:89–96. [PubMed: 11814561]
3. Wu F, Zhang Y, Sun B, McMahon AP, Wang Y. Hedgehog signalling: from basic biology to cancer therapy. *Cell Chem Biol.* 2017; 24:252–280. [PubMed: 28286127]
4. Riobo NA, Manning DR. Pathways of signal transduction employed by vertebrate Hedgehogs. *Biochem J.* 2007; 403:369–79. [PubMed: 17419683]
5. Robbins DJ, Fei DL, Riobo NA. The Hedgehog signal transduction network. *Sci Signal.* 2012; 5(246):re6. [PubMed: 23074268]
6. Riobo NA, Saucy B, Dilizio C, Manning DR. Activation of heterotrimeric G proteins by Smoothened. *Proc Natl Acad Sci USA.* 2006; 103:12607–12. [PubMed: 16885213]
7. Ogden SK, Fei DL, Schilling NS, Ahmed YF, Hwa J, Robbins DJ. G protein Galphai functions immediately downstream of Smoothened in Hedgehog signalling. *Nature.* 2008; 456:967–70. [PubMed: 18987629]
8. Shen F, Cheng L, Douglas AE, Riobo NA, Manning DR. Smoothened is a fully competent activator of the heterotrimeric G protein G(i). *Mol Pharmacol.* 2013; 83:691–7. [PubMed: 23292797]
9. Goodrich LV, Milenkovic L, Higgins KM, Scott MP. Altered neural cell fates and medulloblastoma in mouse patched mutants. *Science.* 1997; 277:1109–13. [PubMed: 9262482]
10. Johnson RL, Rothman AL, Xie J, Goodrich LV, Bare JW, Bonifas JM, Quinn AG, Myers RM, Cox DR, Epstein EH Jr, Scott MP. Human homolog of patched, a candidate gene for the basal cell nevus syndrome. *Science.* 1996; 272:1668–71. [PubMed: 8658145]
11. Fleet A, Lee JP, Tamachi A, Javeed I, Hamel PA. Activities of the Cytoplasmic Domains of Patched-1 Modulate but Are Not Essential for the Regulation of Canonical Hedgehog Signaling. *J Biol Chem.* 2016; 291:17557–68. [PubMed: 27325696]
12. Lu X, Liu S, Kornberg TB. The C-terminal tail of the Hedgehog receptor Patched regulates both localization and turnover. *Genes Dev.* 2006; 20:2539–51. [PubMed: 16980583]
13. Chen XL, Chinchilla P, Fombonne J, Ho L, Guix C, Keen JH, Mehlen P, Riobo NA. Patched-1 proapoptotic activity is downregulated by modification of K1413 by the E3 ubiquitin-protein ligase Itchy homolog. *Mol Cell Biol.* 2014; 34:3855–66. [PubMed: 25092867]
14. Mille F, Thibert C, Fombonne J, Rama N, Guix C, Hayashi H, Corset V, Reed JC, Mehlen P. The Patched dependence receptor triggers apoptosis through a DRAL-caspase-9 complex. *Nat Cell Biol.* 2009; 11:739–46. [PubMed: 19465923]
15. Gibert B, Mehlen P. Dependence receptors and cancer: addiction to trophic ligands. *Cancer Res.* 2015; 75:5171–5. [PubMed: 26627011]

16. Chinchilla P, Xiao L, Kazanietz MG, Riobo NA. Hedgehog proteins activate pro-angiogenic responses in endothelial cells through non-canonical signalling pathways. *Cell Cycle*. 2010; 9:570–79. [PubMed: 20081366]
17. Tanida I. Autophagosome formation and molecular mechanism of autophagy. *Antiox Redox Signal*. 2011; 14:2201–14.
18. Galluzzi L, Baehrecke EH, Ballabio A, Boya P, Bravo-San Pedro JM, Cecconi F, Choi AM, Chu CT, Codogno P, Colombo MI, Cuervo AM, Debnath J, Deretic V, Dikic I, Eskelinen EL, Fimia GM, Fulda S, Gewirtz DA, Green DR, Hansen M, Harper JW, Jäättelä M, Johansen T, Juhasz G, Kimmelman AC, Kraft C, Ktistakis NT, Kumar S, Levine B, Lopez-Otin C, Madeo F, Martens S, Martinez J, Melendez A, Mizushima N, Münz C, Murphy LO, Penninger JM, Piacentini M, Reggiori F, Rubinsztein DC, Ryan KM, Santambrogio L, Scorrano L, Simon AK, Simon HU, Simonsen A, Tavernarakis N, Toozé SA, Yoshimori T, Yuan J, Yue Z, Zhong Q, Kroemer G. Molecular definitions of autophagy and related processes. *EMBO J*. 2017; 36:1811–1836. [PubMed: 28596378]
19. Mizushima N. The role of the Atg1/Ulk1 complex in autophagy regulation. *Curr Opin Cell Biol*. 2010; 22:132–9. [PubMed: 20056399]
20. Russell RC, Tian Y, Yuan H, Park HW, Chang YY, Kim J, Kim H, Neufeld TP, Dillin A, Guan KL. Ulk1 induces autophagy by phosphorylating Beclin-1 and activating VPS34 lipid kinase. *Nat Cell Biol*. 2013; 15:741–50. [PubMed: 23685627]
21. Ichimura Y, Kirisako T, Takao T, Satomi Y, Shimonishi Y, Ishihara N, Mizushima N, Tanida I, Kominami E, Ohsumi M, Nosa T, Ohsumi Y. A ubiquitin-like system mediates protein lipidation. *Nature*. 2000; 408:488–92. [PubMed: 11100732]
22. Polizio AH, Chinchilla P, Chen X, Kim S, Manning DR, Riobo NA. Heterotrimeric Gi proteins link Hedgehog signaling to activation of Rho small GTPases to promote fibroblast migration. *J Biol Chem*. 2011; 286:19589–96. [PubMed: 21474452]
23. Kar R, Singha PK, Venkatachalam MA, Saikumar P. A Novel Role for MAP1 LC3 in Non-Autophagic Cytoplasmic Vacuolation Death of Cancer Cells. *Oncogene*. 2009; 28:2556–68. [PubMed: 19448671]
24. Thompson HG, Harris JW, Wold BJ, Flin F, Brody JP. p62 overexpression in breast tumors and regulation by prostate-derived Ets factor in breast cancer cells. *Oncogene*. 2003; 22:2322–2333. [PubMed: 12700667]
25. Suzuki H, Kaizuka T, Mizushima N, Noda NN. Structure of the Atg101-Atg13 complex reveals essential roles of Atg101 in autophagy initiation. *Nat Struct Mol Biol*. 2015; 22:572–80. [PubMed: 26030876]
26. Qi S, Kim DJ, Stjepanovic G, Hurley JH. Structure of the human Atg13-Atg101 HORMA heterodimer: an interaction Hub within the ULK1 complex. *Structure*. 2015; 23:1848–57. [PubMed: 26299944]
27. Jimenez-Sanchez M, Menzies FM, Chang Y-Y, Simecek N, Neufeld TP, Rubinsztein DC. The Hedgehog signalling pathway regulates autophagy. *Nat Commun*. 2012; 3:1200. [PubMed: 23149744]
28. Pampliega O, Orhon I, Patel B, Sridhar S, Diaz-Carretero A, Beau I, Codogno P, Satir B, Satir P, Cuervo AM. Functional interaction between autophagy and ciliogenesis. *Nature*. 2013; 502:194–200. [PubMed: 24089209]
29. Kim YM, Jung CH, Seo M, Kim EK, Park JM, Bae SS, Kim DH. mTORC1 phosphorylates UVRAG to negatively regulate autophagosome and endosome maturation. *Mol Cell*. 2015; 57:207–18. [PubMed: 25533187]
30. Hausmann G, von Mering C, Basler K. The Hedgehog signalling pathway: where did I come from? *PLoS Biol*. 2009; 7:e1000146. [PubMed: 19564910]
31. Jayaraman SS, Rayhan DJ, Hazany S, Kolodney MS. Mutational landscape of basal cell carcinomas by whole-exome sequencing. *J Invest Dermatol*. 2013; 154:213–220.

IMPLICATIONS

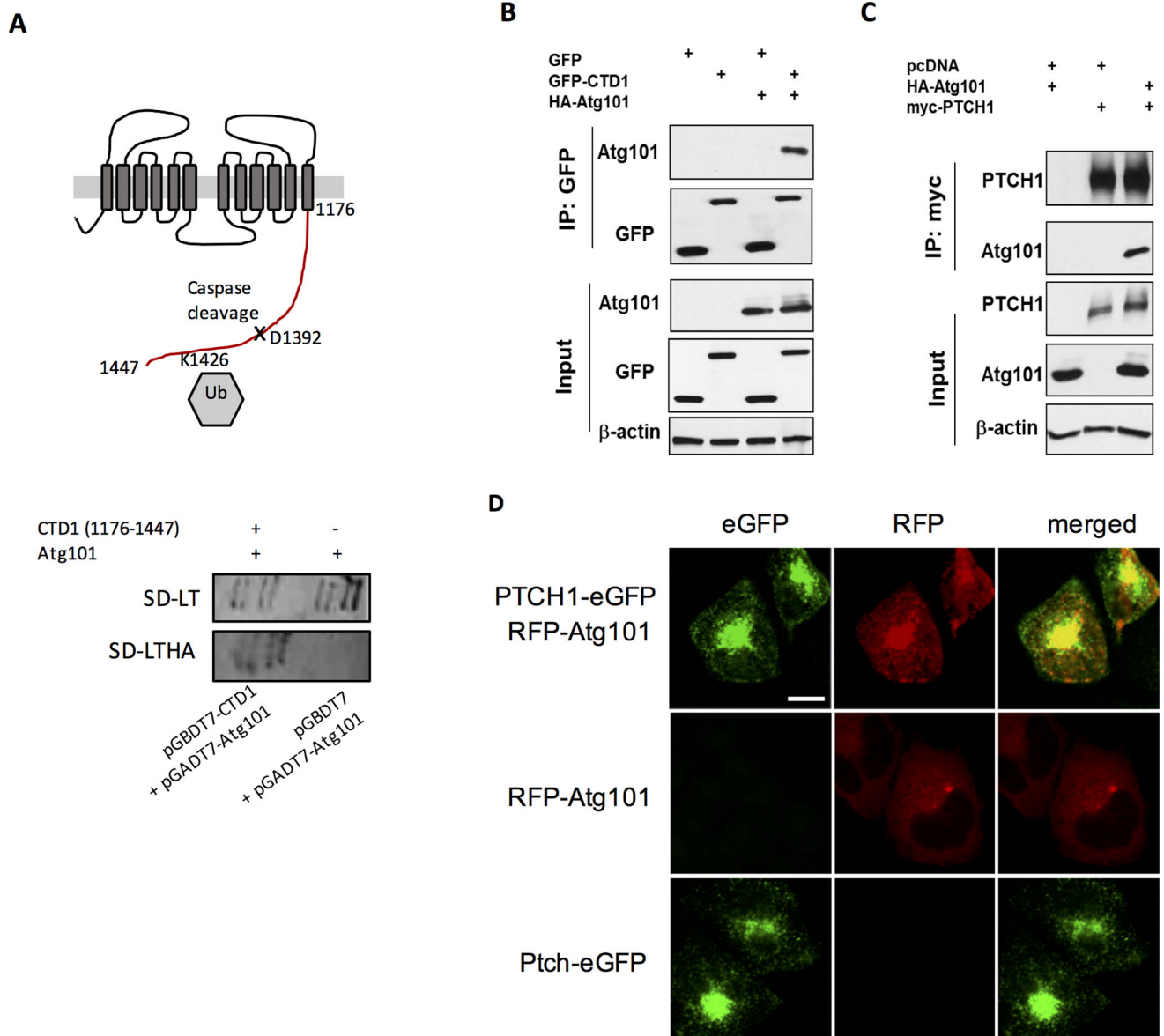
Loss-of-function of the tumor suppressor Patched1 might promote cancer cell fitness by increasing autophagic flux in response to metabolic or environmental stresses.

Author Manuscript

Author Manuscript

Author Manuscript

Author Manuscript

**Figure 1.**

The C-terminal domain of PTCH1 physically interacts with ATG101. **A.** Schematic representation of PTCH1 topological structure, with the cytoplasmic CTD in red and relevant modification sites. Yeast-two-hybrid complementation assay of pGBKT7-CTD1 or empty pGBKT7 with pGADT7-Atg101(1-167) in synthetically-defined (SD) medium without Leu and Trp (SD-LT) and in SD without Leu, Trp, His, and supplemented with Aureobasidin A (SD-LTHA). The backbone of pGBKT7 and pGADT7 encode Trp and Leu biosynthesis genes, respectively; but expression of His biosynthesis gene and AurA resistance is driven by GAL4-responsive UAS promoters of different sequence. **B.** HEK 293 cells were transfected with HA-ATG101 and myr-GFP-CTD1 or empty myr-EGFP. After 24 h, cells were lysed and GFP was immunoprecipitated with an anti-GFP antibody, followed by analysis of HA-ATG101 in the IP and the total lysate (input). **C.** HEK 293 cells were transfected with full length myc-PTCH1 and HA-Atg101. After 24 h, cells were lysed and

PTCH1 was immunoprecipitated with an anti-myc antibody, followed by analysis of HA-ATG101 in the IP and the total lysate (input). **D.** Co-localization of PTCH1-eGFP (green) and RFP-ATG101 (red) in COS-1 cells. Scale bar = 20 mm.

Author Manuscript

Author Manuscript

Author Manuscript

Author Manuscript

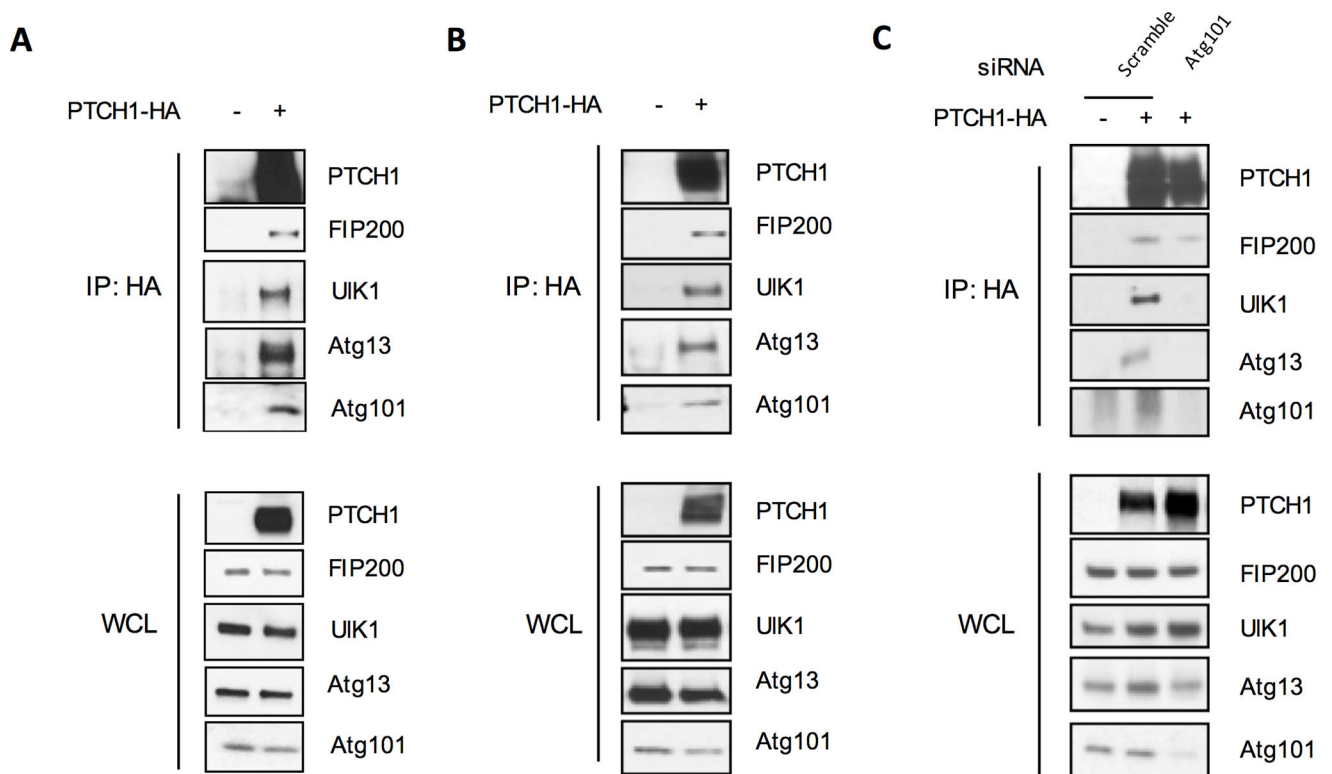
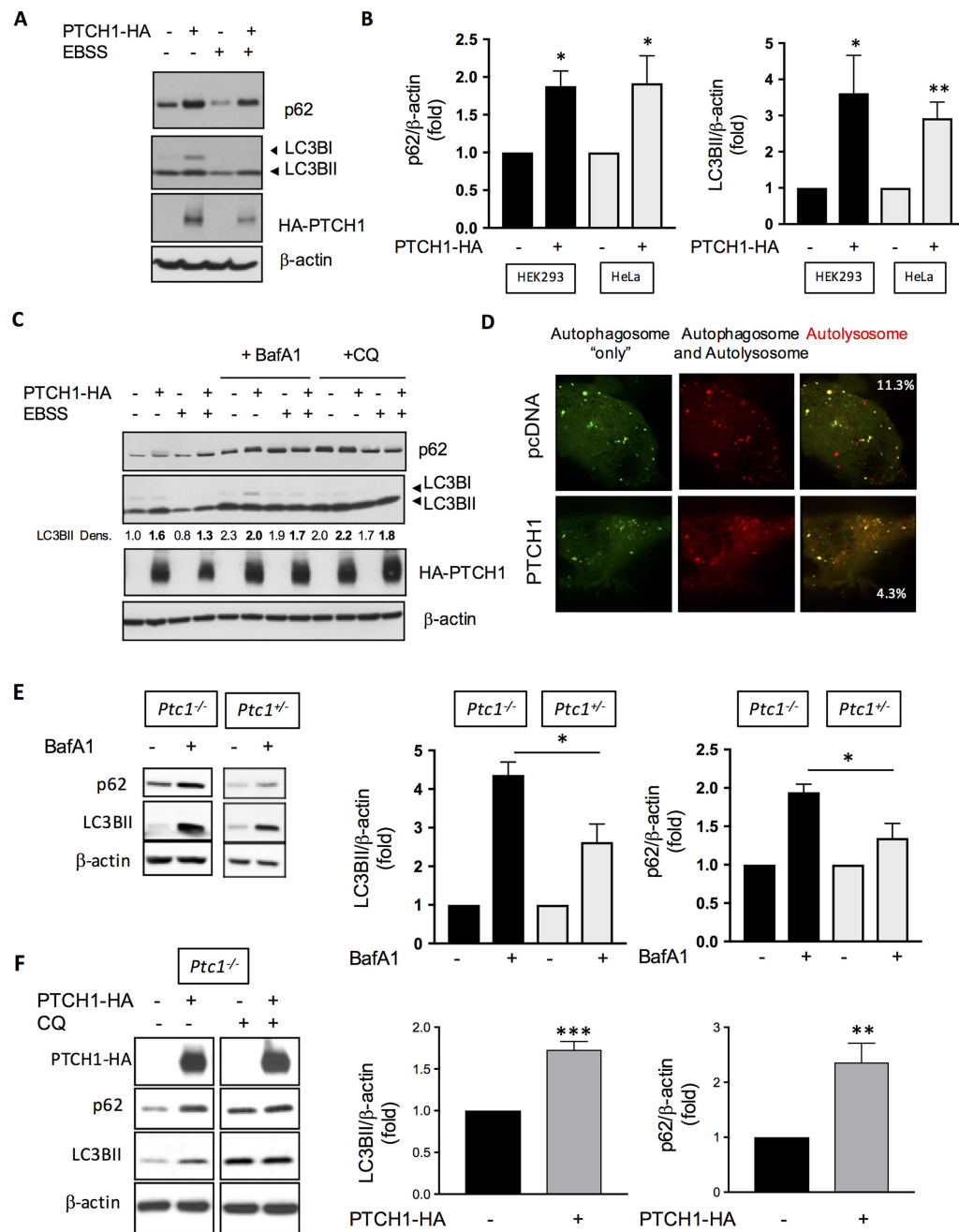


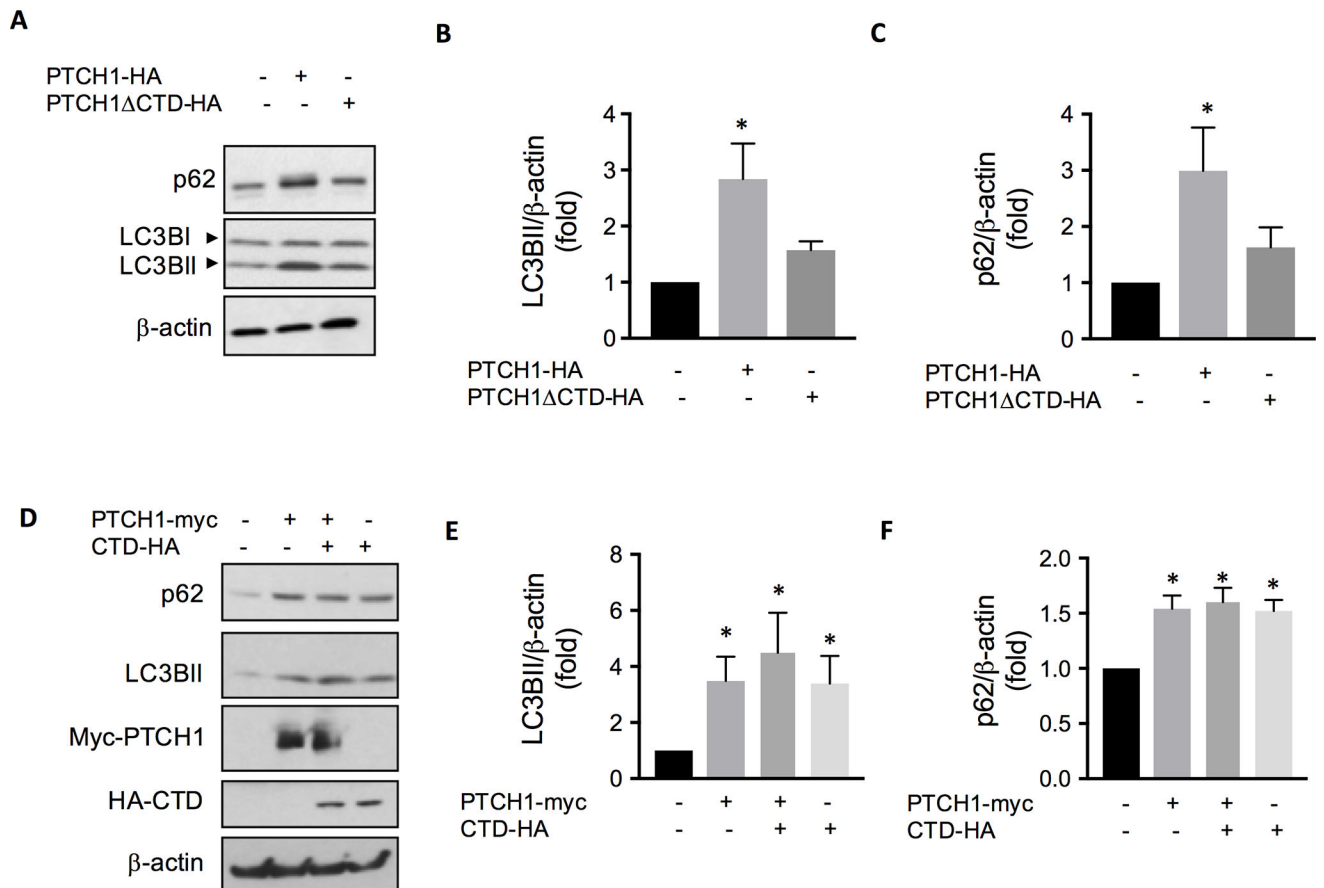
Figure 2.

PTCH1 interacts with the ULK complex via ATG101. **A.** Analysis of endogenous levels of FIP200, ULK1, ATG13, and ATG101 in HA-immunoprecipitates of HEK 293 cells transfected with HA-PTCH1 or empty plasmid in comparison to their expression level in whole cell lysates (WCL). **B.** Same as A but in HeLa cells. **C.** HEK 293 cells were transfected with and *ATG101*-targeting siRNA duplex or with scramble siRNA. 24 h later empty pcDNA3.1 or PTCH1-HA encoding plasmid were transfected as described. Following additional 24 h, cells were lysed and immunoprecipitation (IP) of PTCH1-HA was performed, followed by analysis of endogenous levels of FIP200, ULK1, ATG13, and ATG101 in the IP and the WCL. All experiments were repeated at least 3 times.

**Figure 3.**

PTCH1 impairs completion of autophagy. **A.** Expression levels of p62 and LC3B in HEK 293 cells transfected with pcDNA3.1 or PTCH1-HA and cultured 24 h in complete growth medium or 20 h in complete medium followed by 4 h in minimal EBSS. **B.** Densitometric quantification of p62 and LC3BII western blot signals and normalized to β-actin in HEK 293 and HeLa cells transfected with empty plasmid or PTCH1-HA (n = 5; * P < 0.05. ** P < 0.001). **C.** Expression levels of p62 and LC3B in HEK 293 cells transfected with pcDNA3.1 or PTCH1-HA and cultured 24 h in complete growth medium, without or with addition of 100 nM Bafilomycin A1 (BafA1) or 10 μM chloroquine (CQ) during the last 4 h.

Representative experiment of $n = 3$. Densitometric quantification of LC3BII/ β -actin is indicated under the blot, bold numbers correspond to PTCH1-HA overexpressing cells. **D.** Live imaging in the red and green channels of COS-1 cells expressing the tandem RFP-GFP-LC3B reporter and transfected with pcDNA3.1 or PTCH1-HA. Numbers in the overlay images indicate the percentage of red-only vesicles (autolysosomes) over total (red and green plus red only) vesicles (autolysosomes plus autophagosomes), the difference is statistically significant ($n=3$, $P<0.05$, Student's t-test). Vesicles were counted in at least 10 individual cells in three independent experiments. **E.** Expression levels of p62 and LC3B in *Ptc1^{-/-}* and *Ptc1^{+/-}* MEFs after 4 h in EBSS without or with addition of 100 nM Bafilomycin A1 (BafA1). Representative experiment of $n = 3$. Densitometric quantification of LC3BII and p62 western blot signals normalized to β -actin in *Ptc1^{-/-}* (black bars) and *Ptc1^{+/-}* MEFs (gray bars) ($n = 3$; * $P < 0.05$). **F.** Expression levels of p62 and LC3B in *Ptc1^{-/-}* MEFs transfected with pcDNA3.1 or PTCH1-HA and cultured 24 h in complete growth medium, without or with addition of 10 μ M chloroquine (CQ) for the last 4 h. Representative experiment of $n = 3$. Densitometric quantification of LC3BII and p62 western blot signals normalized to β -actin in pcDNA3.1-transfected (black bars) or PTCH1-HA transfected (gray bars) *Ptc1^{-/-}* MEFs ($n = 3$; ** $P < 0.01$; *** $P < 0.001$).

**Figure 4.**

The CTD of PTCH1 is necessary for autophagic flux inhibition. **A.** Expression levels of p62 and LC3B in HEK 293 cells transfected with pcDNA3.1, PTCH1-HA, or PTCH1 Δ CTD-HA, cultured 24 h in complete growth medium. **B.** Densitometric quantification of LC3BII levels normalized to β -actin in cells transfected as in A (n = 3; * P < 0.05). **C.** Densitometric quantification of p62 levels normalized to β -actin in cells transfected as in A (n = 3; * P < 0.05). **D.** Expression levels of p62 and LC3B in HeLa cells transfected with pcDNA3.1, PTCH1-myc, CTD-HA or PTCH1-myc plus CTD-HA, cultured 24 h in complete growth medium. **E.** Densitometric quantification of LC3BII levels normalized to β -actin in cells transfected as in D (n = 3; * P < 0.05). **F.** Densitometric quantification of p62 levels normalized to β -actin in cells transfected as in D (n = 3; * P < 0.05).

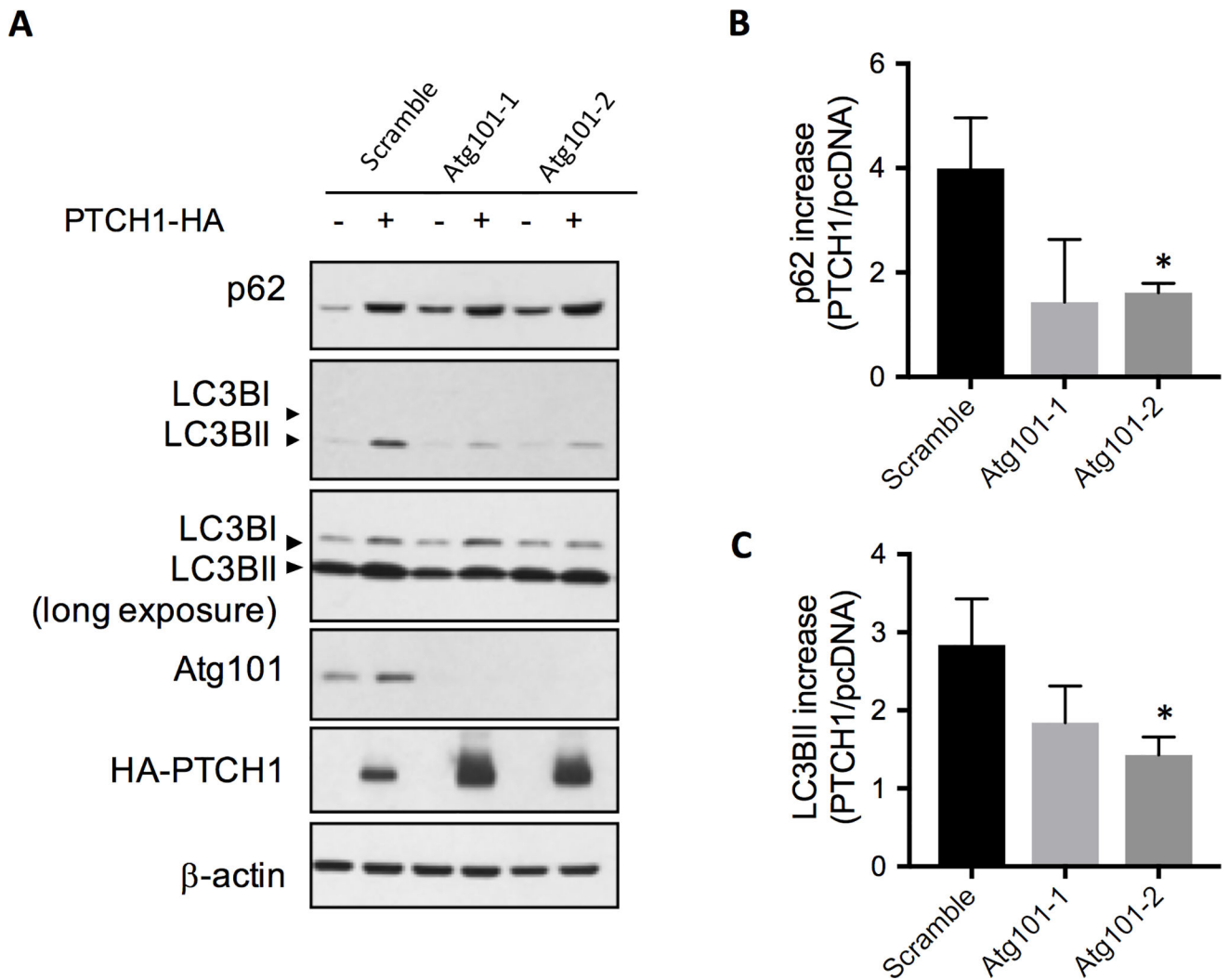


Figure 5. Silencing of ATG101 expression attenuates autophagic flux blockade by PTCH1. **A.** HEK 293 cells were transfected with 2 independent siRNA duplexes targeting Atg101 (Atg101-1 and Atg101-2) or with scramble siRNA. 24 h later empty pcDNA3.1 or PTCH1-HA encoding plasmid were transfected as described. After 24 h, cells were lysed and the levels of p62, LC3B, Atg101, PTCH1-HA and β -actin were determined by western blot. **B.** Densitometric quantification of p62 levels in PTCH1-expressing cells over empty plasmid, for each siRNA condition (n=3; * P<0.05). **C.** Quantification of LC3BII levels in PTCH1-expressing cells over empty plasmid, for each siRNA condition (n=3; * P<0.05).

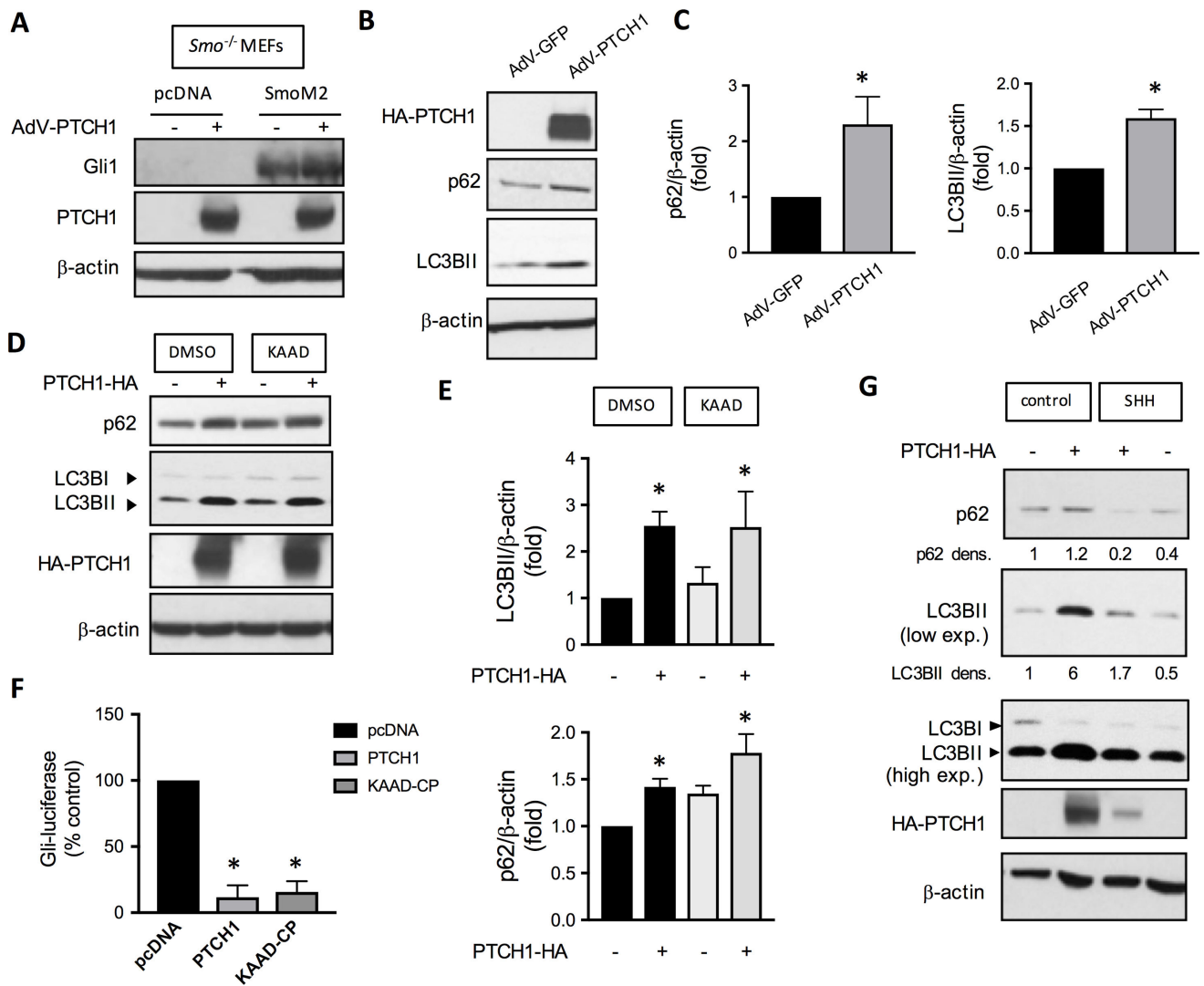


Figure 6. PTCH1 blocks autophagy completion independently of Smoothed. **A.** *Smo*^{-/-} MEFs stably transfected with empty plasmid (pcDNA) or a constitutively active mutant (SmoM2) were transduced with adenovirus encoding PTCH1-HA (AdV-PTCH1) or a control adenovirus (AdV-lacZ). Cells were allowed to grow to confluency, the growth media was replaced by 0.5% FBS-containing DMEM for 24 h, then lysed and the expression level of endogenous Gli1, HA-PTCH1, and β-actin were determined by western blot. **B.** *Smo*^{-/-} MEFs stably transfected with SmoM2 were transduced with AdV-PTCH1 or a control AdV-GFP and 24 h later lysed for western blot analysis of p62 and LC3B levels. **C.** Quantification of p62 and LC3BII levels in cells treated as in B (n=3; * P<0.05). **D.** HEK 293 cells were transfected with empty plasmid or PTCH1-HA and 24 h later treated with 0.5 μM KAAD-cyclopamine (KAAD) or DMSO for additional 24 h. The level of p62 and LC3B expression was interrogated by western blot. **E.** Densitometric quantification of p62 and LC3BII levels normalized to β-actin in cells incubated in DMSO (black bars) or KAAD-cyclopamine (gray bars) as in D (n=3; * P <0.05). **F.** *Ptc1*^{-/-} MEFs were transfected with empty plasmid or PTCH1-HA together with 8XGli-(*Firefly*) luciferase and TK-(*Renilla*)

luciferase reporters. After reaching confluency, serum was reduced from 10% to 0.5% for 24 h and supplemented with 0.5 μ M KAAD-cyclopamine (KAAD-CP) or vehicle. Luciferase activities were determined using the Dual Luciferase Assay as described in Materials and Methods. Data are presented as percent inhibition of the control (n=3; * P< 0.0001 by ANOVA). **G.** HEK 293 cells were transfected with empty plasmid alone, PTCH1-HA, PTCH1-HA and SHH, or SHH alone. After 24 h, the expression level of p62 and LC3B were evaluated by western blot (n=3). Densitometric quantification of the band intensities normalized to β -actin is indicated under the blots.

Author Manuscript

Author Manuscript

Author Manuscript

Author Manuscript